Native-oxide limited cross-plane thermal transport in suspended silicon membranes revealed by scanning thermal microscopy

A. Massoud, J.-M. Bluet, V. Lacatena, M. Haras, J.F. Robillard, Pierre-Olivier Chapuis

Applied Physics Letters

Native-oxide limited cross-plane thermal transport in suspended silicon membranes revealed by scanning thermal microscopy

Cite as: Appl. Phys. Lett. **111**, 063106 (2017); https://doi.org/10.1063/1.4997914
Submitted: 17 May 2017 • Accepted: 26 July 2017 • Published Online: 09 August 2017

A. M. Massoud, J.-M. Bluet, V. Lacatena, et al.

Native-oxide limited cross-plane thermal transport in suspended silicon membranes revealed by scanning thermal microscopy

A. M. Massoud,[1,2,a)] J.-M. Bluet,[1] V. Lacatena,[3,4] M. Haras,[3] J.-F. Robillard,[3] and P.-O. Chapuis[2]
[1]*Univ. Lyon, Institut des Nanotechnologies de Lyon (INL), CNRS, INSA de Lyon, F-69621 Villeurbanne, France*
[2]*Univ. Lyon, CNRS, INSA-Lyon, Université Claude Bernard Lyon 1, CETHIL UMR5008, F-69621 Villeurbanne, France*
[3]*Univ. Lille, CNRS, Centrale Lille, ISEN, Univ. Valenciennes, UMR 8520-IEMN, F-59000 Lille, France*
[4]*STMicroelectronics, 850, rue Jean Monnet, F-38926 Crolles, France*

(Received 17 May 2017; accepted 26 July 2017; published online 9 August 2017)

By thermally characterizing nanometer-thin suspended silicon membranes with various micrometric lengths in ambient conditions, we determine simultaneously the spatial resolution of our Wollaston-probe scanning thermal microscopy experiment, which probes an area of $(285\,\text{nm})^2$, and the effective thermal conductivity of the membranes of $40\,\text{W.m}^{-1}\text{.K}^{-1}$. This value is smaller than the in-plane thermal conductivity measured using other techniques in vacuum ($\sim 60\,\text{W.m}^{-1}\text{.K}^{-1}$), revealing that both cross-plane and in-plane heat conduction are strongly affected by the native oxide in ambient conditions. This work also underlines that high-thermal conductivity samples can be characterized by scanning thermal microscopy when micro-patterned. *Published by AIP Publishing.* [http://dx.doi.org/10.1063/1.4997914]

In contrast to the usual macroscopic scale where thermal conductivity is geometry-independent, the ability to dissipate heat through conduction is known to depend on the geometry at micro- and nanoscales. In the last two decades, many breakthroughs showed that the thermal conductivity of silicon nanowires (NWs) depends on their diameters[1,2] and on the quality of their surfaces.[3,4] The reduction of the effective thermal conductivity was ascribed to a confinement of the phonons and the induced reduction of their mean free paths. It was further shown that roughening of the surfaces can induce a reduction by a factor of ~100 at room temperature.[3,4] Similar phenomena were observed for suspended nano-membranes (M), where the reduction factor was shown to reach ~20 (Refs. 5–12) at room temperature and to be dependent on rough native oxide.[6] Measurements of the suspended objects are performed in vacuum to avoid losses through their sides due to heat convection. As a result, only axial (NW) or in-plane (M) thermal conductivities are measured in these configurations. In principle, radial (NW) and cross-plane (M) thermal conductivities can be evaluated when the nano-objects are either inserted in a matrix or deposited on top of substrates, but it is then difficult to disentangle the effects of thermal boundary conductances (TBCs) from those of conduction within the volume.

Here, we characterize suspended nanometer-thin silicon membranes of micrometric lengths by scanning thermal microscopy (SThM) in ambient conditions and we show that the measurements are affected by cross-plane conduction. The results indicate that thermal transport is strongly influenced by the sides of the membrane, where the impact of the native oxide can be accurately reproduced alternatively by considering silicon dioxide layers of thickness 1.5 nm or a thermal boundary resistance of $\sim 30 \times 10^{-9}\,\text{m}^2\,\text{K}\,\text{W}^{-1}$.

The results are obtained with the thermoresistive SThM probe made of a metallic resistive Wollaston wire.[13] Different characterization techniques have been used for the thermal investigations of suspended nano-objects, e.g., resistive thermometry[14,15] photothermal reflectance,[7,16] and Raman thermometry.[6,17] SThM[18] does not suffer from metal deposition requirements or from optical diffraction-limited spatial resolution but is known to lose its sensitivity when the thermal conductivity λ of bulk materials under investigation becomes larger than $\sim 10\,\text{W.m}^{-1}\text{.K}^{-1}$.[19] Thermoresistive SThM has been applied to samples with a bulk-like configuration, i.e., locally homogeneous samples,[20] to multilayers,[21] to thin films and graphene-based samples,[22–24] and to samples involving a pattern on the surface.[25,26] Data treatment usually requires standard samples or tedious analysis of the heat flow path,[18] especially when probed geometries become complex involving nanometric or micrometric patterns. A technique involving two scans has been developed by Kim *et al.*[27] to improve the energy balance of the probe used in the thermal analysis. The SThM measurements are often influenced by an unknown thermal contact resistance at the tip-sample contact. An efficient solution to determine this parameter has been proposed recently, involving SThM measurements using successively direct and alternating currents.[28] Other authors quantified their thermal measurements by evaluating first the thermal contact resistance.[29,30]

The inset of Fig. 1 shows the Wollaston SThM self-heated probe with constant Joule power in contact with the suspended silicon membrane of width 10 μm, thickness $t_m = 60$ nm (neglecting the possible presence of native oxide), and length $L = 200\,\mu$m. The geometry involves the suspended thin film, an air gap, a substrate, and lateral sides. The membrane lies 14 μm over the silicon substrate

a)Author to whom correspondence should be addressed: antonin.massoud@insa-lyon.fr

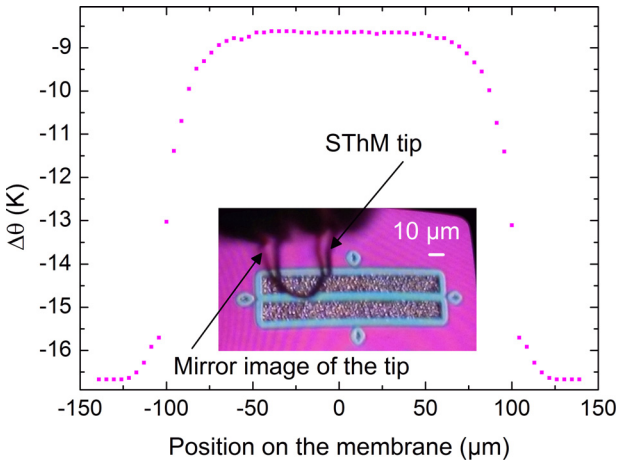

FIG. 1. SThM probe average temperature decrease along the membrane. Inset: Photo of the SThM probe on the suspended membrane (and its mirror image on the sample).

(see Ref. 31 for the fabrication details). While scanning along the membrane, the average temperature decrease of the probe $\Delta\theta = \theta_{tip} - \theta_{far}$ in comparison to its reference value far from contact θ_{far} is recorded (see Fig. 1). $\Delta\theta$ is negative as the tip cools down when the heat flux can dissipate into the sample. A plateau can be observed, which means that the thermal exchange takes place mostly between the probe, the membrane, and the substrate below. Note that no convection can be present as the tip proximity to the membrane does not allow air motion to develop.[32,33] Close to the boundary of the membranes (i.e., over 25 μm on each side), the temperature decrease due to the effect of the sides made of silicon-on-insulator can be observed.

Four different suspended silicon membranes of the same width and same thickness with different lengths $L = 200$, 125, 100, and 75 μm are investigated experimentally. Experimental tip average temperature rises in the plateaus are found to be, respectively, 46.18, 46.10, 45.76, and 45.50 K (vs 54.84 K when the tip is far from contact). From the usual method involving the comparison of the temperature decreases to those in the cases of bulk materials, we find that the fluxes exchanged with the suspended membranes are close to that of homogeneous semi-infinite media of thermal conductivities of the order of 0.3 $W.m^{-1}.K^{-1}$ (see Fig. 2) while a silicon-on-insulator part of the sample is shown to stay close to that of fused quartz (1.3 $W.m^{-1}.K^{-1}$). Note that these estimations consider that the tip-sample thermal contact resistance is identical for all standards and membrane samples. This may appear as a strong approximation at first sight, but the smooth behavior of the calibration curve with the standard samples rules out a non-monotonic impact of this contact resistance, at least in this low effective thermal conductivity range.

A key step in the analysis is to consider a superposition method[33,34] by treating independently the temperature decrease due to dissipation through air $\Delta\theta_{air}$ and the temperature decrease through dissipation at the contact $\Delta\theta_{contact}$: the temperature fields associated are supposed to be independent. The total temperature decrease is $\Delta\theta = \Delta\theta_{air} + \Delta\theta_{contact}$. This separation is possible because the associated temperature fields vary over very different scales ($\sim$10 μm for the air heat conduction,[18] while the contact heat transfer takes place over

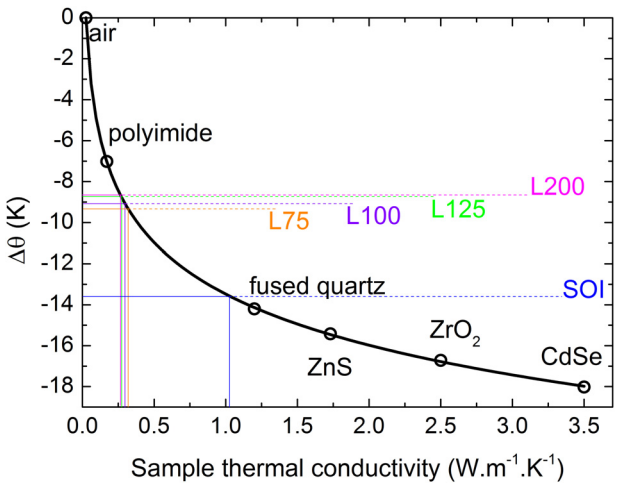

FIG. 2. Experimental data of the difference $\Delta\theta$ between the tip average temperature in contact and far from contact, as a function of the thermal conductivity of standard samples. The temperature differences observed for the membranes can be represented by equivalent thermal conductivities. The black solid line is a guide to the eye.

the nanometer scale). The inset of Fig. 3 shows a 3D FEM simulation of the whole geometry with the tip just before contact (at a height $d_0 = 240$ nm, since diffusion is replaced by ballistic transfer below this distance[33,34]). The average tip temperature decrease due to the air conduction $\Delta\theta_{air}$, with respect to a position far from contact, is represented as a function of the membrane thermal conductivity by the red curve and compared to the case of a tip probing a bulk semi-infinite medium. It can be seen that the probe is still cooled down by high-thermal conductivity membranes by means of the tip-sample heat exchange through air. The technique remains sensitive up to 80 $W.m^{-1}.K^{-1}$ in the case of the membrane, while the sensitivity (slope of the curve) almost vanishes for bulk materials of thermal conductivities larger than 10 $W.m^{-1}.K^{-1}$. This is due to the reduced surface area of the membrane: what matters is the flux exchanged between the heated probe and the membrane. As a result, reducing the

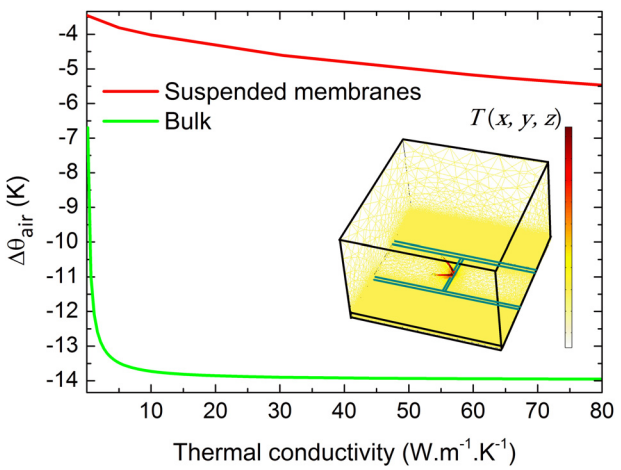

FIG. 3. SThM sensitivity to thermal conductivity highlighted by the tip temperature decrease before contact $\Delta\theta_{air}$ on bulk (green curve) and on suspended membranes (red curve) as a function of sample thermal conductivity. These FEM simulations consider only heat conduction in air. The inset shows the temperature field $T(x,y,z)$ in the heated probe before contact to the suspended membrane and around the probe.

sample area paves the way for the local characterization of high-thermal conductivity materials by scanning thermal microscopy. Note that the tip that was used presents an important tilt with respect to the vertical direction[33] (as shown in Fig. 3), which improves the sensitivity because the tip surface and the sample surface are closer, so the heat exchange through air is stronger. The total sensitivity $\frac{d(\Delta\theta)}{d\lambda} = \frac{d(\Delta\theta_{air})}{d\lambda} + \frac{d(\Delta\theta_{contact})}{d\lambda}$ might be further increased by accounting for the contact contribution $\Delta\theta_{contact}$.

All the investigated membranes are estimated to possess the same thermal conductivity as no dependence on length is expected. The air contribution is simulated with 3D FEM by varying the unknown membrane thermal conductivity $\lambda_{m,test}$. The whole structure is considered as shown in the inset of Fig. 3, and we obtain numerically the tip temperature decrease due to the air transfer channel $\Delta\theta_{air}(\lambda_{m,test})$. In a second step, the contribution of the contact $\Delta\theta_{contact}(\lambda_{m,test})$ is addressed. We do not deal directly with the heat flux exchanged between the tip and the sample surface, but with the same flux when it is dissipated in the sample. In this way, we avoid dealing explicitly with the thermal resistance between the tip and the sample. This means that the thermal contact resistance is considered behaving similarly to the effective thermal conductivity, as observed in Fig. 2. The system {membrane, air cavity, and silicon substrate} is assimilated to a multilayer, of effective thermal conductivity $\lambda_{eff}(\lambda_{m,test})$ modeled with a 2D axisymmetric configuration (see the inset of Fig. 4 and additional explanations in Sec. I in supplementary material). The heat is dissipated from the contact characterized by a disc of radius b. While the tip-sample contact may not be exactly axisymmetric, this is the easiest way to proceed in the absence of experimental evidence for the actual shape. In addition, this simplification is possible because the flux flowing through the contact is not sensitive to the border of the membrane: it is dissipated over a scale much smaller than that of the membrane width (10 μm).

Since $\Delta\theta$ is known experimentally, the abovementioned procedure is equivalent to determining a function $\lambda_{m,test}(b_{test})$. The data are plotted for each membrane, as shown in Fig. 4, and can be fitted linearly. This procedure allows obtaining an effective size for the thermal exchange at contact b and the actual value of the membrane effective thermal conductivity λ_m in the same time. It can be seen that three of the lines converge to the same point while one of the lines is slightly shifted. As a result, we look for the location where the minimum possible dispersion of the total standard deviation is obtained. We obtain $\lambda_m = 39 \pm 3\ \mathrm{W.m^{-1}.K^{-1}}$ (see Fig. 4). We note that the contact radius, $b = 285 \pm 20$ nm, is smaller than usual optical resolutions and may be decreased by dealing with a vertical tip or new-generation SThM involving nano-tips.

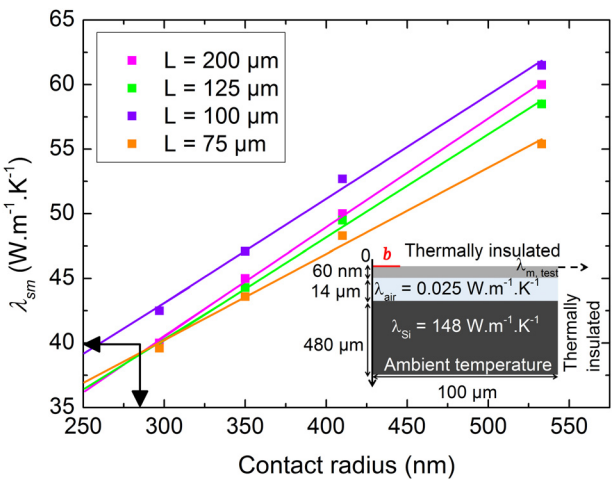

FIG. 4. Membrane effective isotropic thermal conductivity expected as a function of the thermal contact radius. The inset shows the geometry of the multilayer considered below the SThM tip-sample mechanical contact.

The effective thermal conductivity obtained by SThM is smaller than the in-plane data obtained by Raman thermometry ($\lambda_m \sim 60\ \mathrm{W.m^{-1}.K^{-1}}$)[33,35] or with resistive thermometry[31] ($\lambda_m \sim 60\ \mathrm{W.m^{-1}.K^{-1}}$) applied to similar membranes measured in vacuum. The abovementioned analysis does not consider the native oxide SiO_x ($1 < x < 2$) present at both sides of the membranes, of thickness ~1.5 nm,[36] while its effect was shown to be crucial for in-plane transport.[6] An estimation of the associated cross-plane thermal resistance with the thermal conductivity of silica is $\rho_{CP} = t_{SiOx}/\lambda_{SiOx} \sim 10^{-9}\ \mathrm{m^2.K.W^{-1}}$, close to that of the cross-plane transport within the membrane t_m/λ_m. Setting thermal boundary resistances ρ_{CP} on both sides of the membrane in the previous procedure does not change much the isotropic thermal conductivity of the membrane (see the blue curve in Fig. 5). In contrast, by including 1.5 nm SiO_2 layers ($\lambda \sim 1.5\ \mathrm{W.m^{-1}.K^{-1}}$) at the sides of the membranes in the simulations performed to exploit the experimental data, we obtain a silicon isotropic (therefore also in-plane) thermal conductivity of $\sim 59\ \mathrm{W.m^{-1}.K^{-1}}$ in the membrane, in very good agreement with the values determined by the two other techniques and with the ones published in Ref. 9. These results are also in agreement with recent theoretical calculations.[6] In this case, no additional thermal boundary resistance is required at the silicon-silicon oxide and silicon oxide-air boundaries. The nature and structure of the native oxide are known to be very different to those of conventional silica, so this model is very crude. However, it underlines that the thermal transport could be both cross-plane and in-plane in the native oxide.[6] The values of thermal boundary resistance required to reproduce the experimental data in the absence of oxide in volume are analyzed in the supplementary material and found to be $\rho_{TBR} = 29 \pm 2 \times 10^{-9}\ \mathrm{m^2.K.W^{-1}}$, much larger than ρ_{CP}. Slightly different oxide thicknesses are also able to reproduce the experimental data when combined with thermal boundary resistances, but in-plane transport is then anyway required to be considered in the oxide since $\rho_{TBR} \gg \rho_{CP}$. Finally, note that the silicon thermal conductivity in the membrane is probably not isotropic but that it is difficult to consider such anisotropy in the analysis of the experiment.

Our conclusion is that a description where both in-plane and cross-plane transports take place in both the membrane and the native oxide appears sufficient to reproduce the experimental data. These findings should trigger theoretical investigations of the thermal transport in ambient conditions. We are confident that this work will set a strong basis for future quantitative determination of local thermal properties

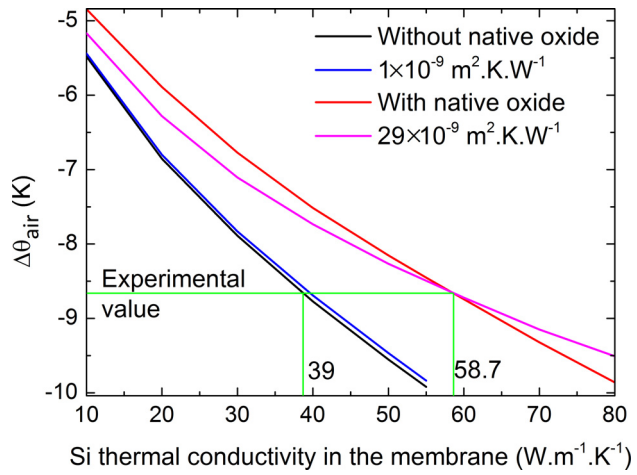

FIG. 5. Tip average temperature decrease computed as a function of the silicon thermal conductivity in the membrane, in the following cases: no contact resistance (see Fig. 4), contact resistances of 10^{-9}K.m^2.W^{-1} and 29×10^{-9}K.m^2.W^{-1}, and native oxide without additional contact resistance.

of nano- and microstructured samples in the cross-plane direction.

See supplementary material for additional details related to the procedure used for determining the effective thermal conductivity from the SThM signal and the uncertainties. We first explain how the configuration can be treated locally as a multilayer and then detail the uncertainties related to both the tip position above the sample in the simulations and the depth of the cavity below the suspended membrane measured experimentally. We provide further details related to the split between the air and the contact contributions and discuss temperatures profiles within and around the membrane. Finally, we give some further explanations related to Fig. 5 and discuss the limitations of the FEM simulations.

The authors acknowledge support from INSA Lyon through BQR project MaNaTherm, from EU projects QuantiHeat and ERC Grant UPTEG 338179, from ANR project NanoHeat, and from project NANO2017. This work was partly supported by the RENATECH French network. We thank Dr. S. Gomes and Dr. S. Lefevre for useful discussions.

[1]D. Li, Y. Wu, P. Kim, L. Shi, P. Yang, and A. Majumdar, Appl. Phys. Lett. **83**, 2934–2936 (2003).
[2]A. I. Boukai, Y. Bunimovich, J. Tahir-Kheli, J.-K. Yu, W. A. Goddard, and J. R. Heath, Nature **451**, 168–171 (2008).
[3]A. I. Hochbaum, R. Chen, R. D. Delgado, W. Liang, E. C. Garnett, M. Najarian, A. Majumdar, and P. Yang, Nature **451**, 163–167 (2008).
[4]J. Lim, K. Hippalgaonkar, S. C. Andrews, and A. Majumdar, Nano Lett. **12**, 2475–2482 (2012).
[5]S. Alaie, D. F. Goettler, M. Su, Z. C. Leseman, C. M. Reinke, and I. El-Kady, Nat. Commun. **6**, 7228 (2015).
[6]S. Neogi, J. S. Reparaz, L. F. C. Pereira, B. Graczykowski, M. R. Wagner, M. Sledzinska, A. Shchepetov, M. Prunnila, J. Ahopelto, C. M. Sotomayor-Torres, and D. Donadio, ACS Nano **9**, 3820–3828 (2015).
[7]M. Nomura, Y. Kage, J. Nakagawa, T. Hori, J. Maire, J. Shiomi, R. Anufriev, D. Moser, and O. Paul, Phys. Rev. B **91**(20), 205422 (2015).
[8]M. Nomura, J. Nakagawa, Y. Kage, J. Maire, D. Moser, and O. Paul, Appl. Phys. Lett. **106**(14), 143102 (2015).
[9]E. Chávez-Ángel, J. S. Reparaz, J. Gomis-Bresco, M. R. Wagner, J. Cuffe, B. Graczykowski, A. Shchepetov, H. Jiang, M. Prunnila, J. Ahopelto, F. Alzina, and C. M. Sotomayor Torres, APL Mater. **2**, 012113 (2014).
[10]P. E. Hopkins, C. M. Reinke, M. F. Su, R. H. Olsson, E. A. Shaner, Z. C. Leseman, J. R. Serrano, L. M. Phinney, and I. El-Kady, Nano Lett. **11**, 107–112 (2011).
[11]J.-K. Yu, S. Mitrovic, D. Tham, J. Varghese, and J. R. Heath, Nat. Nanotechnol. **5**, 718–721 (2010).
[12]J. Tang, H.-T. Wang, D. H. Lee, M. Fardy, Z. Huo, T. P. Russell, and P. Yang, Nano Lett. **10**, 4279–4283 (2010).
[13]R. B. Dinwiddie, R. J. Pylkki, and P. E. West, *Thermal Conductivity*, edited by T. W. Tong (Technomics, Lancaster, PA, 1994), Vol. 22, p. 668–677.
[14]T. S. Tighe, J. M. Worlock, and M. L. Roukes, Appl. Phys. Lett. **70**, 2687–2689 (1997).
[15]W. Fon, K. C. Schwab, J. M. Worlock, and M. L. Roukes, Phys. Rev. B **66**, 45302 (2002).
[16]J. A. Malen, K. Baheti, T. Tong, Y. Zhao, J. A. Hudgings, and A. Majumdar, J. Heat Transfer **133**, 081601 (2011).
[17]S. Peŕichon, V. Lysenko, B. Remaki, D. Barbier, and B. Champagnon, J. Appl. Phys. **86**, 4700 (1999).
[18]S. Gomès, A. Assy, and P.-O. Chapuis, Phys. Status Solidi A **212**, 477–494 (2015).
[19]L. David, Ph.D. thesis, INSA Lyon, 2006.
[20]S. Callard, G. Tallarida, A. Borghesi, and L. Zanotti, J. Non-Cryst. Solids **245**, 203–209 (1999).
[21]V. M. Asnin, F. H. Pollak, J. Ramer, M. Schurman, and I. Ferguson, Appl. Phys. Lett. **75**, 1240 (1999).
[22]M. Timofeeva, A. Bolshakov, P. D. Tovee, D. A. Zeze, V. G. Dubrovskii, and O. V. Kolosov, Ultramicroscopy **162**, 42–51 (2016).
[23]G. Hwang and O. Kwon, Nanoscale **8**, 5280–5290 (2016).
[24]K. Yoon, G. Hwang, J. Chung, H. Kim, O. Kwon, K. D. Kihm, and J. S. Lee, Carbon **76**, 77–83 (2014).
[25]S. Gomès, L. David, V. Lysenko, A. Descamps, T. Nychyporuk, and M. Raynaud, J. Phys. D: Appl. Phys. **40**, 6677–6683 (2007).
[26]B. A. Nelson and W. P. King, Rev. Sci. Instrum. **78**, 023702 (2007).
[27]K. Kim, J. Chung, G. Hwang, O. Kwon, and J. S. Lee, ACS Nano **5**, 8700–8709 (2011).
[28]F. Menges, P. Mensch, H. Schmid, H. Riel, A. Stemmer, and B. Gotsmann, Nat. Commun. **7**, 10874 (2016).
[29]J. Bodzenta, J. Juszczyk, A. Kaźmierczak-Bałata, P. Firek, A. Fleming, and M. Chirtoc, Int. J. Thermophys. **37**, 73 (2016).
[30]A. A. Wilson, M. M. Rojo, B. A. Mayor, J. A. Perez, J. Maiz, J. Schomacker, M. M. Gonzalez, D. A. Borca-Tasciuc, and T. Borca-Tasciuc, Nanoscale **7**, 15404–15412 (2015).
[31]M. Haras, V. Lacatena, T. M. Bah, S. Didenko, J.-F. Robillard, S. Monfray, T. Skotnicki, and E. Dubois, IEEE Electron Device Lett. **37**, 1358–1361 (2016).
[32]X. J. Hu, A. Jain, and K. E. Goodson, Int. J. Therm. Sci. **47**, 820–824 (2008).
[33]A. M. Massoud, Ph.D. thesis, INSA Lyon, 2016.
[34]A. M. Massoud, J.-M. Bluet, and P.-O. Chapuis, "Air contribution in calibrated microprobe-based scanning thermal microscopy," (submitted).
[35]V. Lacatena, Ph.D. thesis, Université de Lille, 2016.
[36]M. Morita, T. Ohmi, E. Hasegawa, and A. Teramoto, Jpn. J. Appl. Phys., Part 1 **29**(12), L2392–L2394 (1990).